THE JOURNAL OF PHYSICAL CHEMISTRY A
A JOURNAL OF THE AMERICAN CHEMICAL SOCIETY

pubs.acs.org/JPCA Article

Probing the Electronic Manifold of MgCl with Millimeter-Wave Spectroscopy and Theory: $(3)^2\Sigma^+$ and $(4)^2\Sigma^+$ States

Published as part of The Journal of Physical Chemistry A special issue "Richard J. Saykally Festschrift".

T. J. Herman, R. Ravi, M. S. Schuurman, N. J. DeYonker, R. W. Field, and L. M. Ziurys*

Cite This: https://doi.org/10.1021/acs.jpca.4c05458 Read Online

ACCESS | Metrics & More | Article Recommendations | Supporting Information

ABSTRACT: The millimeter/submillimeter spectrum of magnesium chloride (MgCl) has been observed in two new electronic excited states, $(3)^2\Sigma^+$ and $(4)^2\Sigma^+$, using direct absorption methods. The molecule was synthesized in a mixture of Cl_2, argon, and magnesium vapor. For the $(3)^2\Sigma^+$ state, multiple rotational transitions were measured in the $v = 0$ level for all six isotopologues ($^{24}Mg^{35}Cl$, $^{24}Mg^{37}Cl$, $^{25}Mg^{35}Cl$, $^{25}Mg^{37}Cl$, $^{26}Mg^{35}Cl$, and $^{26}Mg^{37}Cl$), as well as up to $v = 13$ for $^{24}Mg^{35}Cl$. For the $(4)^2\Sigma^+$ state, less intense spectra were recorded for $^{24}Mg^{35}Cl$ ($v = 0-2$). Equilibrium rotational parameters were determined for both states for $^{24}Mg^{35}Cl$, as well as rotational constants and ^{25}Mg hyperfine parameters for the other isotopologues. A perturbation was observed between rotational levels of the two states due to an avoided crossing. Computations were also carried out at the CASPT2 and MRCISD+Q levels, and the resulting bond lengths for $(3)^2\Sigma^+$ and $(4)^2\Sigma^+$ states agree well with the experimental values of $r_e = 2.536$ and 2.361 Å. The computations show that the $(3)^2\Sigma^+$ state has a double-well potential; however, the state behaves as a single well with unperturbed vibrational levels up to $v = 13$ due to nonadiabatic interactions with the $(4)^2\Sigma^+$ state.

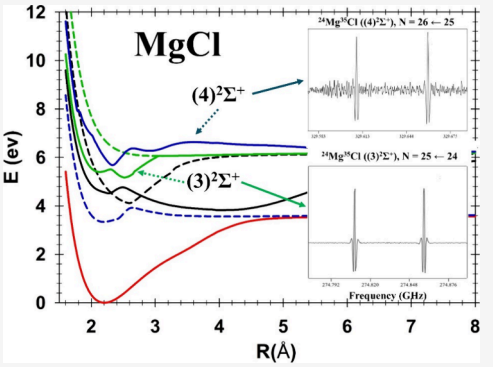

INTRODUCTION

The recent discovery that the lowest energy quantum states of diatomic molecules can be selectively populated via laser cooling has renewed spectroscopic interest in metal monohalide molecules.[1,2] These species are known to have several excited states with strong diagonal Franck−Condon factors to their ground electronic state, making them relevant for laser cooling experiments[3−5] and condensed phase physics.[6] Further investigation of excited states of such species will present new targets for these ultracold investigations. With proven success in alkaline earth monohalide case studies of SrF and CaF, other likely species are BaF and MgF, which have seen recent theoretical and experimental interest.[7−10] Analogous to MgF, the heavier MgCl will likewise be a good candidate for such experiments, and investigations into its electronic state manifold will determine whether it is suitable for laser cooling.

MgCl has been the subject of numerous spectroscopic studies[11,12] with applications in materials science[13−15] and astronomy.[16] Its ground state has been investigated via rotational spectroscopy, including detailed spectral analysis of its isotopologues.[17−19] The lowest excited electronic states have also been explored, with studies conducted for the $A^2\Pi$-$X^2\Sigma^+$[20−22] and $B^2\Sigma^+$-$A^2\Pi$[23,24] bands. Any states higher in energy than the $B^2\Sigma^+$ state have yet to be observed experimentally.

Several states of MgCl have also been investigated via ab initio methods, with emphasis on their adiabatic and diabatic natures.[25−31] Calculations have been performed, for example, at the MRCI level for the $(2)^2\Pi$ and other higher excited electronic states. However, these studies do not agree in the details of the electronic manifold above the $(2)^2\Pi$ state in energy, such as the potential well shapes for the excited Σ states.

Here we present a pure rotational study of two new excited electronic states of MgCl, coupled with computational work at the CASPT2 and MRCISD+Q levels, which has led to their identification as the $(3)^2\Sigma^+$ and $(4)^2\Sigma^+$ states. This study offers new insight into the complexity of the excited electronic states of this radical. In this work, rotational spectra have been recorded for each of the six isotopologues of the $(3)^2\Sigma^+$ state of MgCl ($^{24}Mg^{35}Cl$, $^{24}Mg^{37}Cl$, $^{25}Mg^{35}Cl$, $^{25}Mg^{37}Cl$, $^{26}Mg^{35}Cl$, and $^{26}Mg^{37}Cl$) in the ground vibrational state, for multiple ($v = 1-13$) vibrationally excited states of $^{24}Mg^{35}Cl$, and for $v = 0$, 1, and 2 of the $(4)^2\Sigma^+$ state of $^{24}Mg^{35}Cl$. The computational effort that aided in the assignment of these states is also described.

Received: August 14, 2024
Revised: October 23, 2024
Accepted: October 25, 2024

Table 1. Selected Rotational Transitions for Isotopologues of $(3)^2\Sigma^+$ MgCl[a]

		$^{24}Mg^{35}Cl$ $v = 0$		$^{24}Mg^{37}Cl$ $v = 0$		$^{26}Mg^{35}Cl$ $v = 0$		$^{26}Mg^{37}Cl$ $v = 0$	
$N' \leftarrow N''$	$J' \leftarrow J''$	ν_{obs}	$\nu_{obs-calc}$	ν_{obs}	$\nu_{obs-calc}$	ν_{obs}	$\nu_{obs-calc}$	ν_{obs}	$\nu_{obs-calc}$
19 ← 18	18.5 ← 17.5	208971.582	0.004						
	19.5 ← 18.5	209021.297	0.009						
20 ← 19	19.5 ← 18.5	219952.269	−0.010	215130.116	0.010				
	20.5 ← 19.5	220001.960	−0.008	215178.727	−0.001				
21 ← 20	20.5 ← 19.5	230930.037	−0.001	225867.644	−0.005	220426.025	0.002	215362.590	−0.002
	21.5 ← 20.5	230979.702	−0.005	225916.247	−0.002	220473.437	−0.001	215408.899	−0.030
25 ← 24	24.5 ← 23.5	274808.726	0.004	268786.883	0.008	262313.766	−0.005		
	25.5 ← 24.5	274858.295	0.001	268835.381	0.007	262361.098	0.001		
26 ← 25	25.5 ← 24.5	285769.572	0.003	279508.236	−0.006	272777.659	−0.012	266514.730	−0.002
	26.5 ← 25.5	285819.116	0.002	279556.711	−0.001	272824.984	0.011	266560.973	0.001
27 ← 26	26.5 ← 25.5	296726.597	0.004	290225.954	0.003	283238.088	0.001	276735.718	0.019
	27.5 ← 26.5	296776.113	0.004	290274.389	−0.003	283285.363	−0.001	276781.920	0.003
28 ← 27	27.5 ← 26.5	307679.635	−0.010	300939.861	−0.001	293694.885	−0.001	286953.230	0.019
	28.5 ← 27.5	307729.131	−0.002	300988.272	−0.001	293742.124	−0.012	286999.412	0.005
29 ← 28	28.5 ← 27.5					304147.940	0.006	297167.150	0.006
	29.5 ← 28.5					304195.157	0.001	297213.314	−0.002
		$^{24}Mg^{35}Cl$ $v = 1$		$^{24}Mg^{35}Cl$ $v = 2$		$^{24}Mg^{35}Cl$ v = 3		$^{24}Mg^{35}Cl$ v = 4	
$N' \leftarrow N''$	$J' \leftarrow J''$	ν_{obs}	$\nu_{obs-calc}$	ν_{obs}	$\nu_{obs-calc}$	ν_{obs}	$\nu_{obs-calc}$	ν_{obs}	$\nu_{obs-calc}$
19 ← 18	18.5 ← 17.5								
	19.5 ← 18.5								
20 ← 19	19.5 ← 18.5	218501.816	0.000	217057.788	−0.016	215620.310	0.006	214189.272	0.009
	20.5 ← 19.5	218550.813	−0.005	217106.116	−0.011	215667.930	0.003	214236.190	0.010
21 ← 20	20.5 ← 19.5	229407.057	−0.004			226381.498	0.004	224878.923	0.011
	21.5 ← 20.5	229456.036	−0.005			226429.086	−0.009	224925.797	−0.009
25 ← 24	24.5 ← 23.5	272995.752	0.021	271190.826	−0.003	269394.011	−0.015	267605.316	−0.004
	25.5 ← 24.5	273044.606	−0.004	271239.019	0.007	269441.537	0.012	267652.118	0.003
26 ← 25	25.5 ← 24.5	283884.101	0.016	282007.006	−0.014	280138.361	−0.008	278278.146	0.002
	26.5 ← 25.5	283932.948	0.011	282055.164	−0.008	280185.830	−0.010	278324.916	0.006
27 ← 26	26.5 ← 25.5	294768.614	−0.007	292819.403	0.006	290878.901	−0.002	288947.176	0.012
	27.5 ← 26.5	294817.442	−0.001	292867.528	0.012	290926.344	−0.001	288993.903	0.002
28 ← 27	27.5 ← 26.5	305649.179	−0.011	303627.810	−0.004	301615.496	0.015	299612.228	−0.005
	28.5 ← 27.5	305697.977	−0.006	303675.889	−0.010	301662.892	0.001	299658.935	−0.006
29 ← 28	28.5 ← 27.5								
	29.5 ← 28.5								

[a]In MHz.

EXPERIMENTAL SECTION

The pure rotational spectra of MgCl in the $(3)^2\Sigma^+$ and $(4)^2\Sigma^+$ states were recorded using one of the millimeter/submillimeter direct absorption spectrometers of the Ziurys group. The instrument is composed of a coherent and tunable source of mm and submm radiation, a gas cell that incorporates a Broida-type oven, and a detector system. Several Gunn oscillators, which operate in the range of 65−140 GHz, serve as the basic sources for the spectrometer; higher frequencies are achieved using Schottky diode multipliers. The radiation is directed from a scalar feedhorn, through a wire grid, and focused into the cell quasi-optically using several Teflon lenses. At the back of the cell is a rooftop reflector, which passes the radiation back though the cell after rotating its plane of polarization. The radiation is then reflected from a wire grid into the detector, an InSb bolometer, which is cooled to ∼4 K with liquid helium. Phase-sensitive detection at $2f$ is achieved through FM modulation of the source and the use of a lock-in amplifier. The spectrometer is controlled with a computer via an IEEE bus. Additional details of the instrument are described elsewhere.[32]

Rotational transitions from the new states of magnesium chloride were observed while attempting a survey from 260 to 300 GHz for another molecule (HMgCl) in the presence of Mg vapor (generated in the oven) with an Ar carrier, and H_2 and Cl_2 gases. The optimal partial pressures and oven temperatures varied, but the signal-to-noise was typically maximized using 1−5 mTorr of argon carrier gas, introduced from below the oven, with <1 mTorr of Cl_2 added to the flowing gas mixture from above the oven. A green glow was observed over the oven when conducting the experiment.

The frequencies of the spectra were recorded by scanning both in increasing and decreasing frequency, and the resulting data were then averaged. Center frequencies for transitions were determined by fitting Gaussian curves to the line profiles, and typical line widths were 430−1100 kHz over the range 210−460 GHz. In total, 319 lines were recorded with this method. Six to eight rotational transitions were measured for each isotopologue in the $v = 0$ vibrational states. Frequencies of higher vibrational states ($v \geq 5$) of $^{24}Mg^{35}Cl$ were extracted from a single 100 MHz scan and are not as accurate.

https://doi.org/10.1021/acs.jpca.4c05458
J. Phys. Chem. A XXXX, XXX, XXX−XXX

Table 2. Selected Rotational Transitions for $(3)^2\Sigma^{+25}$MgCl ($v = 0$)[a]

			$^{25}Mg^{35}Cl$		$^{25}Mg^{37}Cl$	
$N' \leftarrow N''$	$J' \leftarrow J''$	$F' \leftarrow F''$	ν_{obs}	$\nu_{obs-calc}$	ν_{obs}	$\nu_{obs-calc}$
22 ← 21	21.5 ← 20.5	19 ← 18	236172.846	−0.058	230869.750	−0.028
		20 ← 19	236174.421	−0.031	230871.361	−0.050
		21 ← 20	236176.056	−0.011	230872.984	−0.032
		22 ← 21	236177.652	−0.005	230874.626	0.065
		23 ← 22	236178.661	−0.376	230875.856	−0.070
		24 ← 23	236179.354	−0.243	230876.143	−0.456
	22.5 ← 21.5	24 ← 23	236215.012	0.070	230910.105	−0.283
		23 ← 22	236215.496	0.079	230911.110	0.089
		22 ← 21	236216.571	−0.071	230912.555	0.178
		21 ← 20	236218.205	0.116	230914.094	0.181
		20 ← 19	236219.786	0.139	230915.735	0.249
		25 ← 24	236221.354	−0.061	230917.153	−0.009
25 ← 24	24.5 ← 23.5	22 ← 21	268299.201	−0.071	262276.636	0.016
		23 ← 22	268300.558	−0.032	262277.972	−0.035
		24 ← 23	268301.880	−0.048	262279.295	−0.047
		25 ← 24	268303.096	−0.096	262280.572	−0.004
		26 ← 25	268304.322	0.134	262281.672	0.106
		27 ← 26	268304.653	0.331	262282.033	0.254
	25.5 ← 24.5	27 ← 26	268342.492	−0.359	262318.782	−0.084
		26 ← 25	268342.805	−0.116	262319.034	−0.014
		25 ← 24	268343.829	0.032	262320.084	0.053
		24 ← 23	268345.029	0.079	262321.320	0.062
		23 ← 22	268346.324	0.082	262322.650	0.083
		28 ← 27	268347.683	−0.048	262323.961	−0.026
27 ← 26	26.5 ← 25.5	24 ← 23	289699.476	−0.078	283197.983	−0.021
		25 ← 24	289700.715	−0.030	283199.190	−0.066
		26 ← 25	289701.891	−0.043	283200.382	−0.062
		27 ← 26	289703.058	0.031	283201.445	−0.069
		28 ← 27	289703.874	0.041	283202.331	0.014
		29 ← 28	289704.225	0.429	283202.598	0.258
	27.5 ← 26.5	29 ← 28	289743.326	−0.565	283240.709	−0.350
		28 ← 27	289743.651	−0.149	283240.979	−0.077
		27 ← 26	289744.357	−0.147	283241.864	0.011
		26 ← 25	289745.555	0.054	283242.938	0.021
		25 ← 24	289746.704	0.053	283244.089	0.006
		30 ← 29	289747.953	−0.035	283245.279	−0.084

[a]In MHz.

COMPUTATIONS

Potential energy curves were computed via two different approaches. The first employed the complete active space self-consistent field (CASSCF) approach to generate reference state wave functions and energies, which were augmented using second-order perturbation theory corrections to the electronic energies (CASPT2). The active space employed to generate the reference states and energies was an augmented "full-valence" CAS, and included all 9 valence electrons with an additional a_1 orbital (9 total) to cleanly describe molecular dissociation, with the total active space denoted (9,9). A quadruple-ζ atomic natural orbital (ANO) basis set was employed for both the Mg and Cl atoms,[33] denoted ANO-L-VQZP. The OpenMolcas suite was used for all CASSCF/CASPT2 electronic structure computations.[34] In addition, the nonadiabatic coupling was calculated between the $(3)^2\Sigma^+$ and $(4)^2\Sigma^+$ states at the RASSCF level of theory.

Second, state-averaged complete active space self-consistent field (SA-CASSCF) computations were used with the same (9,9) active space described above. In total, 9 A_1, 6 B_1, 6 B_2, and 4 A_2 (in the Abelian C_{2v} point group) electronic states were utilized in the SA-CASSCF expansion. This selection of states corresponds to the first four atomic asymptotes of Mg + Cl. Scalar relativistic effects via correlation consistent basis sets (cc-pwCV5Z-DK on Mg and aug-cc-pwCV5Z-DK on Cl)[35−37] were considered, as well as implementation of the spin-free, second-order, one-electron Douglas−Kroll−Hess (DKH) Hamiltonian. From the SA-CASSCF reference configuration state functions, potential energy curves were computed using internally contracted MRCISD+Q energies with the manifold of doublet A_1 states. The L_z^2 expectation values were confirmed to have integer values for all reported SA-CASSCF results. The Molpro2023.3 software package was used for all SA-CASSCF/MRCISD+Q computations.[38−40]

RESULTS

On scanning the range from 260 to 300 GHz, numerous recurring doublet patterns were immediately observed, with evidence of hyperfine splitting in some of the spectra. The typical doublet splitting was 47−48 MHz. Chemical tests were performed, which showed that the signals required both Mg

https://doi.org/10.1021/acs.jpca.4c05458
J. Phys. Chem. A XXXX, XXX, XXX−XXX

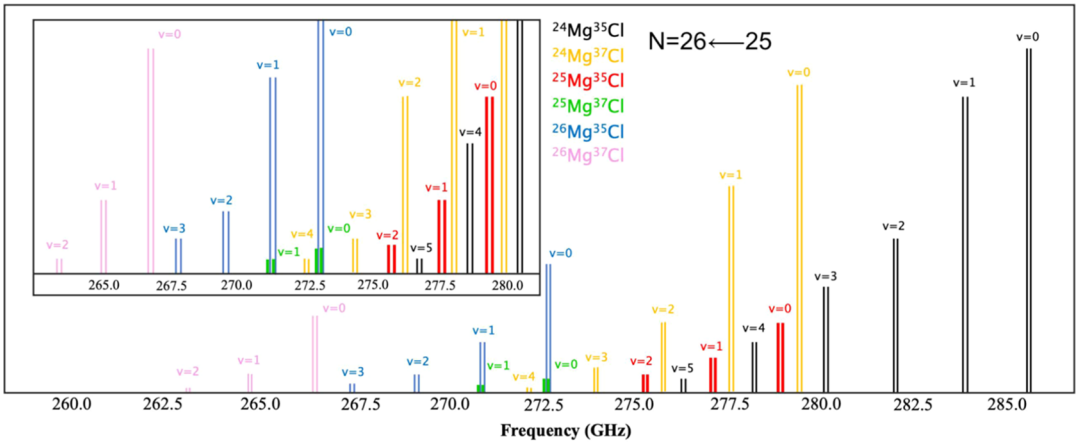

Figure 1. Stick spectrum of the observed spin-rotation doublets of the $N = 26 \leftarrow 25$ rotational transition centered near 272 GHz of the newly identified $(3)^2\Sigma^+$ state of the MgCl radical, showing the assignment of the isotopologues ($^{24}Mg^{35}Cl$, $^{24}Mg^{37}Cl$, $^{25}Mg^{35}Cl$, $^{25}Mg^{37}Cl$, $^{26}Mg^{35}Cl$, and $^{26}Mg^{37}Cl$) and vibrational satellite patterns recorded. The hyperfine splittings of the $^{25}Mg^{35}Cl$ and $^{25}Mg^{37}Cl$ species are collapsed for simplicity. The inset shows less intense transitions, with the *y*-axis scaled to 50% that of the main image. Vibrational satellite lines up to $v = 13$ were recorded in certain transition of the main isotopologues but are not shown for clarity.

vapor and Cl_2. Addition or removal of H_2 did not affect signals, nor did the addition of O_2 and other reactants. Attempts to improve signal strength by application of a DC discharge also proved unsuccessful. Additional surveys were conducted between 210 and 250 GHz and 320−360 GHz to observe additional rotational transitions. The spectral patterns appeared to arise from an electronic state of MgCl, but not the well-studied ground and A or B excited states.

More than three dozen doublet patterns were identified. The most intense, largest rotational constant pattern ($B \sim 5500$ MHz) was assumed to be that of $^{24}Mg^{35}Cl$, the most abundant isotopologue. With this initial assignment, the patterns for many magnesium and chlorine isotopologues were identified. Moreover, the $^{25}Mg^{35}Cl$ and $^{25}Mg^{37}Cl$ patterns contained hyperfine splitting typical of ^{25}Mg ($I = 5/2$) with a characteristic sextet structure. Rotational transitions arising from excited vibrational levels, so-called "satellite lines," were assigned for $v = 1$ up to 13; they followed a classic diatomic pattern where the rotational constant B_v depends linearly on $(v + 1/2)$. All doublets were then assigned. The intensities of each pattern were consistent with the relative abundances of the respective isotopes of magnesium (^{24}Mg, ^{25}Mg, ^{26}Mg = 78.9%, 10.0%, 11.0%) and chlorine (^{35}Cl, ^{37}Cl = 75.8%, 24.2%). The expected decrease in intensity of vibrationally excited rotational transitions with quantum number$v$ was also observed. Six to eight rotational transitions, each consisting of resolved spin-rotation doublets (and, in addition, for the ^{25}Mg species, hyperfine components), were recorded for each isotopologue in their $v = 0$ vibrational state, and two to nine transitions for v = 1 to 13. Representative data are shown in Tables 1 and 2. The complete data sets are presented in the Supporting Information (Tables S1−S4), for up to $v = 4$ with ±50 kHz uncertainty in the measurements and for $v = 5$−13 with ±150 kHz uncertainty.

Figure 1 illustrates the overall observed pattern for the $N = 26 \leftarrow 25$ transition of this excited state, identified as $(3)^2\Sigma^+$. The inset shows some of the weaker features. Note that the figure only shows data for the vibrational satellite lines up to $v = 5$, although lines were observed up to $v = 13$. A representative spectrum of $N + 1 \leftarrow N$ rotational transitions ($N = 25 \leftarrow 24$, $26 \leftarrow 25$, or $27 \leftarrow 26$) of each species $^{24}Mg^{35}Cl$, $^{24}Mg^{37}Cl$, $^{25}Mg^{35}Cl$, $^{25}Mg^{37}Cl$, $^{26}Mg^{35}Cl$, $^{26}Mg^{37}Cl$ are shown in Figure 2. The spin-rotation doublets are clearly visible in each spectrum, as well as the sextet hyperfine pattern in the two ^{25}Mg isotopologes (middle panels), labeled F_1 to F_6 for simplicity. This designation corresponds to $F_{1\cdots6} = J - I, J - I + 1, \ldots, J + I$. Note that the F_6 and F_5 components are blended in the lower frequency spin-doublet and also in the F_4 and F_5 components in the higher frequency one. There is also overlap of the upper spin component of $^{25}Mg^{37}Cl$ and the lower component of $^{26}Mg^{35}Cl$, indicated by an asterisk in the lower middle panel. Other contaminating lines are also marked by asterisks.

While searching the 320−360 GHz range for higher transitions of the $(3)^2\Sigma^+$ electronic state (above $N = 28$), a separate set of doublet patterns with a similar splitting of 48−50 MHz was identified, but a distinctly different rotational constant ($B \sim 6350$ MHz). These features were ~60 times less intense, and only the $v = 1$ and 2 satellite lines were observed. The new, weaker pattern first appeared for the $N = 26 \leftarrow 25$ transition and at higher N. Six to seven transitions each were measured for this electronic state in the $v = 0$, 1, and 2 vibrational levels. Sample data are shown in Table 3. Sample spectra of this electronic state, $(4)^2\Sigma^+$, are shown in Figure 3. Here the successive $N = 26 \leftarrow 25$, $N = 27 \leftarrow 26$, and $N = 28 \leftarrow 27$ transitions are displayed. The spin-rotation doublets are apparent in each spectrum. Two additional lines visible in the $N = 27 \leftarrow 26$ spectrum, marked by asterisks, arise from a spin-doublet of an isotopologue of MgCl in the ground state.

The stronger, $(3)^2\Sigma^+$ pattern abruptly disappeared at the $N = 29 \leftarrow 28$ transition in all vibrational levels up to at least $v = 7$. Although the $v = 0$ lines could not be measured due to source limitations (multiplier frequency coverage), the $v = 5$ and 6 lines could be accessed. Despite significant signal averaging, these transitions could not be observed at the predicted frequency or within a few 100 MHz of it. Searches for higher N transitions ($N = 31 \leftarrow 30$ through $N = 34 \leftarrow 33$) also proved unsuccessful. In contrast, the less intense $(4)^2\Sigma^+$ state was visible from starting with the $N = 26 \leftarrow 25$ transition and could be traced up to $N = 37 \leftarrow 36$, which is the practical limit of the spectrometer tuning range. Searches for lower N lines ($N = 24 \leftarrow 23$ and below) were unsuccessful, as

https://doi.org/10.1021/acs.jpca.4c05458
J. Phys. Chem. A XXXX, XXX, XXX−XXX

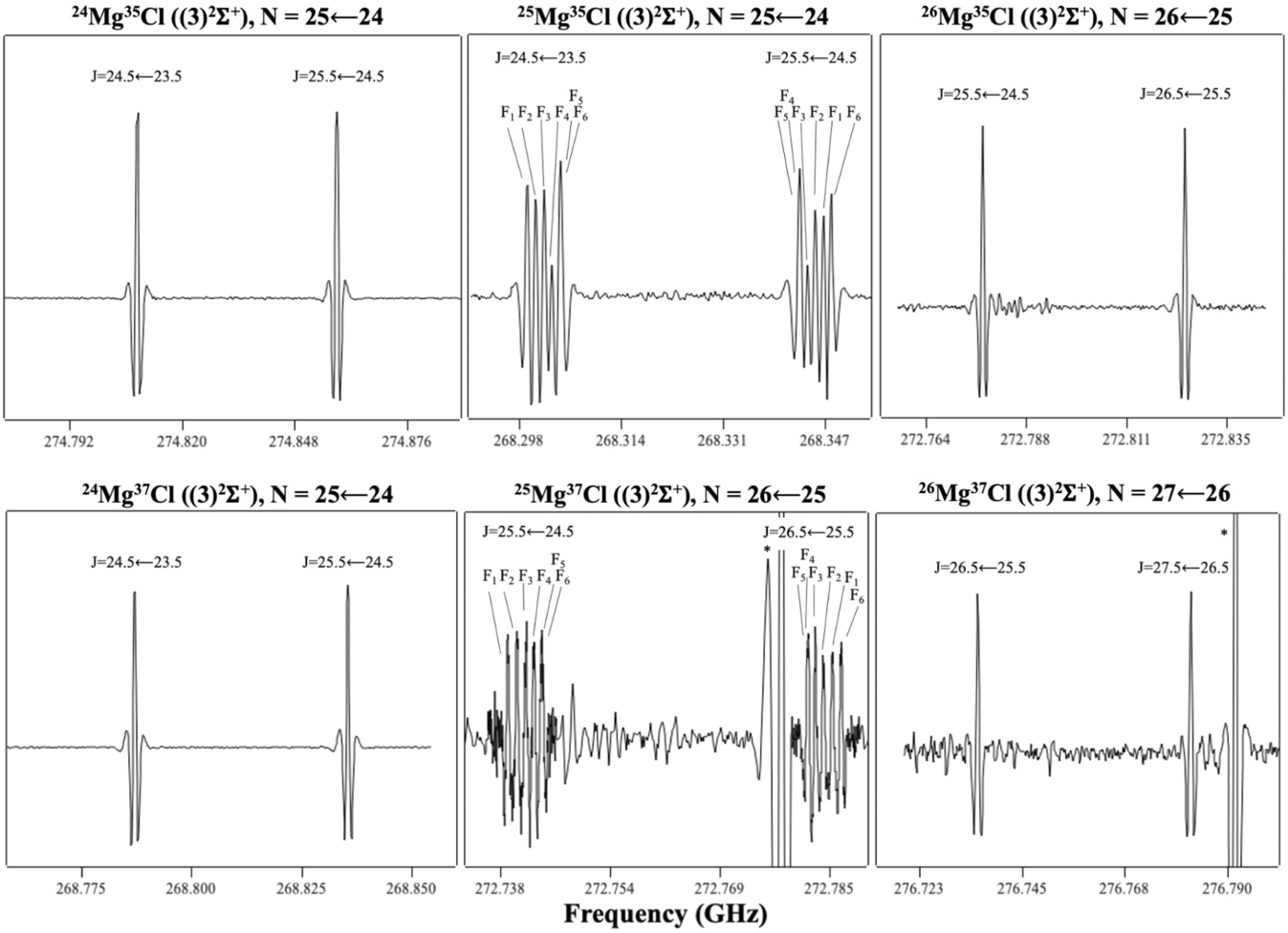

Figure 2. Measured spectra of rotational transitions of the six isotopologues of MgCl ($(3)^2\Sigma^+$). In the left panels, the $N = 25 \leftarrow 24$ transition of the $^{24}Mg^{35}Cl$ and $^{24}Mg^{37}Cl$ isotopologues are shown, measured near 274.8 and 268.8 GHz; in the middle are the same transition of the $^{25}Mg^{35}Cl$ and the $N = 26 \leftarrow 25$ of the $^{25}Mg^{37}Cl$ species, measured near 268.3 and 272.7 GHz, and on the right are the $N = 26 \leftarrow 25$ and $N = 27 \leftarrow 26$ transitions of $^{26}Mg^{35}Cl$ and $^{26}Mg^{37}Cl$, respectively, measured near 272.8 and 276.8 GHz. The sextet hyperfine structure pattern, labeled by the F quantum number (labeled simply F_{1-6} for clarity), is evident in the ^{25}Mg data and is indicated above the spectra. For each spin doublet, the inner hyperfine components were collapsed, resulting in partially blended lines. There is an overlap of the upper spin component of $^{25}Mg^{37}Cl$ and the lower component of $^{26}Mg^{35}Cl$ (center lower panel), designated with an asterisk. Also marked with an asterisk is a contaminant line in the bottom right panel. Each spectrum is of a continuous region, created from two 40 s, ∼60 MHz-wide scans.

Table 3. Selected Rotational Transitions for $(4)^2\Sigma^+ {}^{24}Mg^{35}Cl$[a]

		$v = 0$		$v = 1$		$v = 2$	
$N' \leftarrow N''$	$J' \leftarrow J''$	ν_{obs}	$\nu_{obs-calc}$	ν_{obs}	$\nu_{obs-calc}$	ν_{obs}	$\nu_{obs-calc}$
26 ← 25	25.5 ← 24.5	329609.245	−0.017	327416.912	−0.007	325234.414	−0.035
	26.5 ← 25.5	329658.791	−0.004	327465.467	−0.019	325282.007	0.007
27 ← 26	26.5 ← 25.5	342245.801	0.017	339969.197	0.030	337702.805	0.007
	27.5 ← 26.5	342295.270	−0.006	340017.696	0.007	337750.287	−0.022
28 ← 27	27.5 ← 26.5	354877.581	−0.001	352516.687	−0.012	350166.449	0.012
	28.5 ← 27.5	354927.028	−0.003	352565.164	−0.011	350213.919	0.010
29 ← 28	28.5 ← 27.5	367504.483	0.001	365059.327	−0.013	362625.222	0.028
	29.5 ← 28.5	367553.903	0.017	365107.793	0.025	362672.632	0.009

[a]In MHz.

mentioned. These perturbed patterns, illustrated in Figure 4, clearly represent two separate electronic states of MgCl.

The theoretical calculations at the CASPT2 level generated the electronic state manifold shown in Figure 5. The experimentally studied $X^2\Sigma^+$, $A^2\Pi$ and $B^2\Sigma$ (also called $(2)^2\Sigma^+$) states are visible, as well as the higher lying $(3)^2\Sigma^+$, $(2)^2\Pi$, $(4)^2\Sigma^+$, and $(1)^2\Sigma^-$ states. The $(3)^2\Sigma^+$ and $(4)^2\Sigma^+$ states both have a double potential well and an avoided crossing. The vertical black and red dotted lines show the experimental bond lengths of the $(3)^2\Sigma^+$ and $(4)^2\Sigma^+$ states, as derived below. The bond distances identify them as the first "outer" well in the $(3)^2\Sigma^+$state nearer to the dissociation limit,

https://doi.org/10.1021/acs.jpca.4c05458
J. Phys. Chem. A XXXX, XXX, XXX−XXX

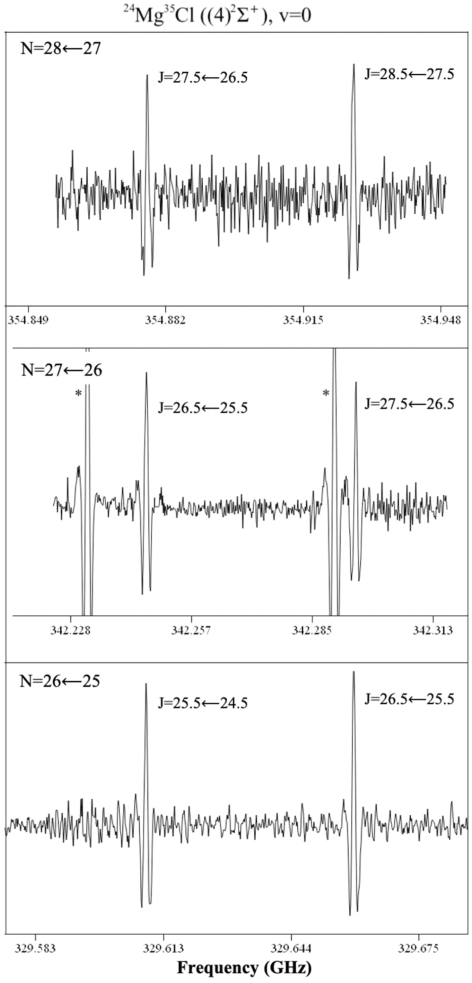

Figure 3. Spectra of rotational transitions of $^{24}Mg^{35}Cl$ in the $(4)^2\Sigma^+$ state. The $N = 26 \leftarrow 25$, $N = 27 \leftarrow 26$, and $N = 28 \leftarrow 27$ transitions are shown for the $v = 0$ state, recorded near 329.6, 342.2, and 354.9 GHz, respectively. A spin-doublet of an isotopologue of MgCl in the ground state is indicated by an asterisk. Each spectrum is of a continuous region, formed from two 40 s, ∼60 MHz-wide scans.

and the second, "inner" well for the $(4)^2\Sigma^+$ state; they lie ∼5−6 eV above the ground state. Theoretical equilibrium bond distances, harmonic vibrational constants ω_e and dissociation energies were also computed at the CASPT2 and MRCISD+Q levels. The larger (9,9) active space used in the present calculations matches that employed in ref 31, but not ref 30, where the authors used a smaller active space and missed the observed $(4)^2\Sigma^+$ state.

■ ANALYSIS

For the $(3)^2\Sigma^+$ state, six isotopologues in $v = 0$ through 4 for $^{24}Mg^{35}Cl$ were fit to an effective Hamiltonian in a Hund case (b) basis. For the $(4)^2\Sigma^+$ state, the $v = 0$, 1, and 2 data were analyzed for $^{24}Mg^{35}Cl$. The following Hamiltonian was used, with the latter two terms used for the two species with ^{25}Mg:

$$\mathbf{H}_{eff} = \mathbf{H}_{rot} + \mathbf{H}_{sr} + \mathbf{H}_{mhf} + \mathbf{H}_{eQq} \quad (1)$$

The molecular hyperfine terms considered were Fermi contact, b_F, dipolar interaction c, and the quadrupole coupling eQq.[41] Note that there was no evidence in the spectra for chlorine hyperfine interactions; both isotopes have $I = 3/2$. The least-squares fitting routine SPFIT[42] was used for the analysis. The molecular constants determined (B, D, γ, and γ_D) are listed in Table 4 for $^{24}Mg^{35}Cl$ in the $(3)^2\Sigma^+$ ($v = 0-4$) and $(4)^2\Sigma^+$ ($v = 0-2$) states, and in Table 5 for the other five isotopologues ($(3)^2\Sigma^+$). Also included are the ground state constants for MgCl from Bogey et al.[17] The rms of the fits ranged from 5 to 26 kHz for all species except $^{25}Mg^{35}Cl$ and $^{25}Mg^{37}Cl$, where it was 186−209 kHz, a result of the blending of hyperfine components. In the latter cases, both b_F and c were determined, but eQq was fitted only for $^{25}Mg^{35}Cl$. Note that successive inclusion of γ_D, c_I, and b_{FD} in the ^{25}Mg fits resulted in undefined parameters at the 3σ level and were therefore not used in the final analysis.

Rotational, centrifugal distortion and spin-rotation constants were determined for the $v = 0-4$ and $v = 0-2$ vibrational levels of the $(3)^2\Sigma^+$ and $(4)^2\Sigma^+$ states, respectively. Equilibrium parameters B_e, α_e, D_e, β_e, γ_e, and γ_e' were derived from linear fits using the classical expresssions.[12] These results are presented in Table 6, along with the computational values. There is excellent agreement between the experimental and theoretical bond lengths—between 1 and 2% at the CASPT2 level. Interestingly, the harmonic spectroscopic constants computed at the MRCISD+Q level of theory give slightly less desirable agreement with experiment. MRCISD+Q is expected to provide a better treatment of dynamical electron correlation. The computed error could be attributed to the more extensive state averaging of the reference CASSCF wave function and orbitals, the chosen active space, and/or the overarching challenge of computing reliable adiabatic spectroscopic constants in a region of the potential energy curve with significant diabatic perturbations.

■ DISCUSSION

Two New Excited Electronic States in MgCl. The electronic ground state of MgCl has been studied thoroughly with a rotational constant of B = 7339.1 MHz and spin-rotation splitting near ∼66 MHz for the main isotopic species ($v = 0$). The rotational constant for the $B^2\Sigma^+$ (also called the $(2)^2\Sigma^+$ state) is B = 7982 MHz. In contrast, the states measured in this work for $^{24}Mg^{35}Cl$ ($v = 0$) have B = 5504.3 and 6349.0 MHz with smaller spin-rotation splitting near 50 MHz. The spectral patterns of the new states clearly indicate $^2\Sigma$ symmetry. Very strong rotational transitions of the ground state were routinely observed among those of the new states, as well. The excellent agreement between the experimental and theoretical bond distances identifies the new electronic excited states of MgCl as $(3)^2\Sigma^+$ and $(4)^2\Sigma^+$.

As shown in Figure 5, both states arise from the Mg (^{3}P) + Cl (^{2}P) atomic asymptotes. The ground atomic state of Mg is ^{1}S. In the Broida oven source, some percentage of gas-phase magnesium must be in the excited metastable ^{3}P state. This state lies ∼2.4 eV above the ground state, and may be populated by some nonthermal process or from excess energy generated in the formation of ground state MgCl. The green fluorescence observed in the reaction mixture is evidence for the presence of the metastable ^{3}P state. Collisions with Cl lead atoms to the formation of the electronic excited states.

The observation of pure rotational spectra, however, in such excited electronic states is unusual. It is expected that decay to the ground $^2\Sigma^+$ state would be rapid. The excited state lifetimes must be long enough such that there is sufficient population in the rotational levels to measure absorption of the millimeter radiation. Based on the relative intensities of the (3) and X

https://doi.org/10.1021/acs.jpca.4c05458
J. Phys. Chem. A XXXX, XXX, XXX−XXX

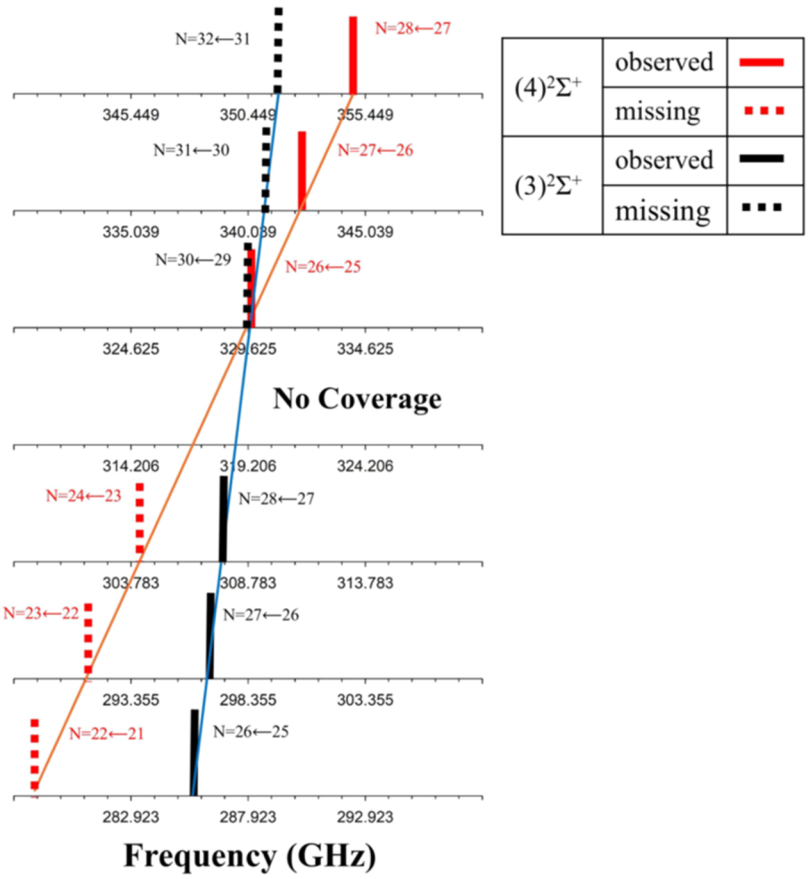

Figure 4. Loomis Wood plot of the rotational patterns of $(3)^2\Sigma^+$ (black) and $(4)^2\Sigma^+$states (red) of $^{24}Mg^{35}Cl$ (v = 0). Each line in the plot represents a doublet pair. The solid lines indicate the observed transitions, while the dotted lines indicate the transitions that were not seen. The blue and orange lines indicate the expected pattern for the rotational transitions of the $(3)^2\Sigma^+$ and $(4)^2\Sigma^+$ states, respectively. The $(3)^2\Sigma^+$ pattern abruptly disappears at N = 29 ← 28 and above; the $(4)^2\Sigma^+$ lines only appear at N = 26 ← 25 and above. The region between 308.3 to 326.8 has no coverage for the v = 0 lines due to source limitations.

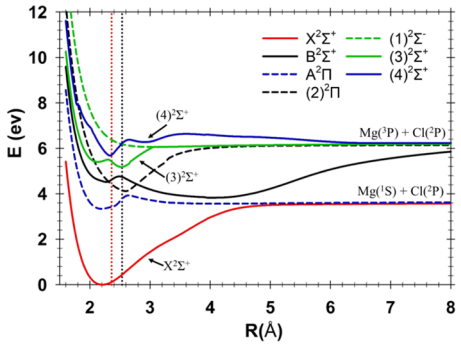

Figure 5. Potential energy curves of $^{24}Mg^{35}Cl$ using the ab initio CASPT2 method. The dotted vertical lines indicate the experimental bond lengths measured in this work. The black dotted line (2.536 Å) corresponds to $(3)^2\Sigma^+$, and the red dotted line (2.361 Å) corresponds to $(4)\ ^2\Sigma^+$. Note the double well potential of the $(3)^2\Sigma^+$ and the $(3)^2\Sigma^+$-$(4)^2\Sigma^+$ avoided crossing.

state rotational lines, which is roughly 1:3, the lifetime of the (3) excited state is estimated to be ∼700 s., assuming collisions of Mg + Cl produce MgCl in a highly uncertain branching ratio of (3):X ∼ 1:10,000.

One possible qualitative explanation for the unusually long lifetime in the (3) and (4) states is the difference in their bonding character relative to the ground state. As discussed below, the (3) state appears to be more covalent than the highly ionic ground state, with more of a Mg^0Cl^0 configuration as opposed to Mg^+Cl^-. Therefore, the transition (3) → X would require moving an electron localized on the magnesium nucleus to an orbital localized on Cl. This kind of charge transfer is unfavorable because there is poor orbital overlap between the initial and final states.

Evidence of the differences in orbital character is found in a comparison of hyperfine parameters of $^{25}Mg^{35}Cl$ for the ground and the $(3)^2\Sigma^+$ states; see Table 5. The Fermi contact (b_F), dipolar (c), and quadrupolar (eQq) terms of the $(3)^2\Sigma^+$ state differ from those of the ground state. The b_F value is smaller (−227.9(2.1) MHz vs −329.1(2.9) MHz) and c has a value of −61.8(9.8) MHz as opposed to 0 MHz. (The c constant simply could not be fit in the ground state data). The quadrupole term is larger as well (−84(41) MHz vs −19.0(1.5) MHz). Although the hyperfine parameters derived depend somewhat on the analysis, the differences would suggest that the unpaired electron in MgCl has ∼47% s-character in the (3) state, as compared to ∼66% in the electronic ground state.[19] This result is consistent with a nonzero dipolar term in the excited state, and the larger eQq term. These hyperfine constants suggest that the (3) state is more covalent than the ground state.

Diabatic $(3)^2\Sigma^+$ Potential and Perturbations in the Spectra. Several computational studies, here and in ref 31, indicate that the $(3)^2\Sigma^+$ state has a double potential well with a second minimum near r_e ∼ 2.1 Å. The energy barrier between

https://doi.org/10.1021/acs.jpca.4c05458
J. Phys. Chem. A XXXX, XXX, XXX−XXX

Table 4. Spectroscopic Parameters for $^{24}Mg^{35}Cl$[a]

state	vibrational level	B	D	γ	γ_D	rms of fit
$X^2\Sigma^+$	$v = 0$[b]	7339.1042(11)	0.0081683(18)	66.516(59)	0.000250(70)	
$(3)^2\Sigma^+$	$v = 0$	5504.33102(33)	0.00612872(27)	49.900(29)	−0.000175(17)	0.006
	$v = 1$	5468.05476(33)	0.00612112(27)	49.221(29)	−0.000182(17)	0.009
	$v = 2$	5431.93924(44)	0.00611270(34)	48.570(40)	−0.000206(21)	0.010
	$v = 3$	5395.98704(41)	0.00610525(32)	47.844(36)	−0.000184(20)	0.008
	$v = 4$	5360.19565(39)	0.00609708(31)	47.136(35)	−0.000182(19)	0.010
$(4)^2\Sigma^+$	$v = 0$	6348.97259(26)	0.00729048(12)	50.064(31)	−0.000262(11)	0.010
	$v = 1$	6306.78776(26)	0.00727931(12)	49.134(31)	−0.000280(11)	0.017
	$v = 2$	6264.79221(24)	0.00726806(11)	48.047(29)	−0.0002445(93)	0.026

[a]Parameters in MHz; stated uncertainties are 3σ. [b]ref 17.

Table 5. Spectroscopic Parameters for $(3)^2\Sigma^+$MgCl Isotopologues[a]

parameter	$^{24}Mg^{37}Cl$	$^{25}Mg^{35}Cl$	$^{25}Mg^{37}Cl$	$^{26}Mg^{35}Cl$	$^{26}Mg^{37}Cl$
B	5383.55006(38)	5373.7721(18)	5252.9776(18)	5253.72695(37)	5132.93222(33)
D	0.00586209(30)	0.0058416(14)	0.0055771(13)	0.00558264(28)	0.00532864(23)
γ	48.841(34)	48.284(78)	47.179(57)	47.625(35)	46.518(30)
γ_D	−0.000183(19)			−0.000159(18)	−0.000137(15)
b_F		−227.9(2.1)	−229.1(1.1)		
c		−61.8(9.6)	−44.9(8.9)		
eQq		−84(41)	−77[b]		
rms of fit	0.005	0.186	0.209	0.009	0.014

[a]Parameters in MHz; stated uncertainties are 3σ. [b]Held fixed; see text.

Table 6. Equilibrium Parameters for $(3)^2\Sigma^+$ and $(4)^2\Sigma^+$$^{24}Mg^{35}Cl$[a]

		$(3)^2\Sigma^+$ ab initio			$(4)^2\Sigma^+$ Ab initio	
parameter	$(3)^2\Sigma^+$experiment	CASPT2	MRCISD+Q	$(4)^2\Sigma^+$ experiment	CASPT2	MRCISD+Q
B_e	5522.03(21)	5596	5885	6369.99(28)	6513	6876
α_e	35.95(18)			42.09(16)		
D_e	0.0061302(84)			0.00729609(11)		
$\beta_e \times 10^6$	−6.52(80)			−11.21(62)		
γ_e	50.263(54)			50.59(23)		
γ_e'	−0.692(16)			−1.01(14)		
r_e (Å)	2.53629(42)	2.519	2.457	2.36145(52)	2.335	2.273
ω_e (cm^{-1})		697	694		1064	1076
D_E (eV)		0.91			0.97	

[a]Parameters in MHz unless specified otherwise; uncertainties are 3σ.

the two wells is roughly coincident with the $v = 4$ level of the observed (3) state, using the theoretical value of ω_e. However, the pure rotational data for the (3) state show no obvious effects of the presence of the second "internal" well, as the external well is characterized up to $v = 13$. Satellite-line spectra measured up to $v = 13$ in several rotational transitions, for example, $N = 28 \leftarrow 27$, show an unperturbed pattern characteristic of a single well. A plot of calculated rotational constants up to $v = 13$ for the (3) state vs $v + 1/2$ is linear, with a correlation coefficient of 0.999, as displayed in Figure 6. There are no obvious deviations from this linear relationship, as might be expected above the double-well barrier.[43] A sample spectrum of the $N = 27 \leftarrow 26$ transition arising from the $v = 13$ level is shown as an inset in Figure 6. The spin-rotation doublets are clearly visible in these data. Searches for the $v = 14$ lines following the given pattern were not successful. Using the theoretical value of ω_e, observation of the $v = 13$ lines is roughly consistent with the theoretical dissociation limit of ~1 eV from the $v = 0$ level of the (3) state to the $Mg(^3P) + Cl(^2P)$ asymptote.

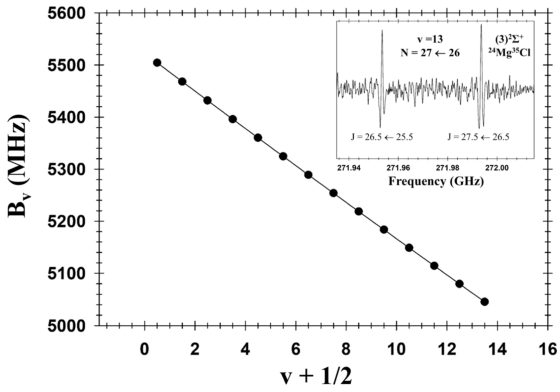

Figure 6. Plot of the measured rotational constants for $(3)^2\Sigma^+$$^{24}Mg^{35}Cl$ from $v = 0$ to $v = 13$ as a function of $v + 1/2$. The trend is clearly linear, with no evidence of perturbations. The inset shows the spin-rotation doublet of the $N = 27 \leftarrow 26$ rotational transition in the $v = 13$ state, measured in a single 100 MHz scan with a duration of 1 min.

https://doi.org/10.1021/acs.jpca.4c05458
J. Phys. Chem. A XXXX, XXX, XXX−XXX

These data suggest that the (3) state follows the diabatic curve of the (4) state as $r < 2.36$ Å, and bypasses the double well. This odd behavior indicates a breakdown of the adiabatic picture. To further explore the $(3)^2\Sigma^+$ and $(4)^2\Sigma^+$ interaction, their nonadiabatic coupling was calculated at the RASSCF level of theory as a function of internuclear distance. The calculated interaction matrix element is sharply peaked near the minimum of the $(4)^2\Sigma^+$ state. (Note that the bond length of the peak is slightly shifted from the CASPT2 minimum). The coupling between these states should be fairly strong, as there is a moderately strong avoided crossing between them. Also, the $B^2\Sigma^+$ ($(2)^2\Sigma^+$) state may also be involved in the overall interaction, as it undergoes an avoided crossing with the (3) state near 2.5 Å; see Figure 5. Clearly, subsequent computations in a vibronic basis are needed to fully understand these data and will be the subject of future work.

The disappearance of the (3) state rotational pattern near $N = 29 \leftarrow 28$ and the appearance of the (4) state near $N = 26 \leftarrow 25$, as shown in Figure 4, can be partly explained by an avoided crossing of the two states. Based on estimates of the energies of the rotational levels using the theoretical ω_e values and the experimental constants, the two states are nearly coincident in energy at the $N = 29$, $v = 7$ levels of the $(3)^2\Sigma^+$ state and at $N = 24$ in the $v = 0$ level of the $(4)^2\Sigma^+$ state. The crossing is qualitatively illustrated in Figure 7. These energies are

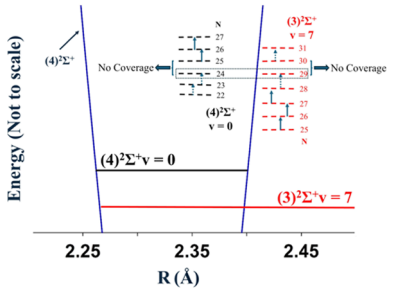

Figure 7. Qualitative picture of the perturbation between the $(3)^2\Sigma^+$ and $(4)^2\Sigma^+$ states, based on the theoretical vibrational and measured rotational constants. The blue trace indicates the $(4)^2\Sigma^+$ potential curve, while rotational levels are shown for the two states in red ($(3)^2\Sigma^+$) and black ($(4)^2\Sigma^+$). Near the $N = 29$ ($v = 7$) rotational level of the $(3)^2\Sigma^+$state and the $N = 24$ ($v = 0$) level of the $(4)^2\Sigma^+$ state, the levels cross, indicated by the dotted rectangle. Observed and "missing" transitions are indicated by solid and dotted arrows. An inaccessible transition is also shown.

approximate, as the level calculations do not include vibrational anharmonicity and are based on computed ω_e values. Also, millimeter sources have insufficient power at certain critical frequencies. There are limited measurements at the adjacent $N = 30 \leftarrow 29$ line of the $(3)^2\Sigma^+$ state ($v = 0$–4) and similarly at the $N = 25 \leftarrow 24$ line of the $(4)^2\Sigma^+$ state. Nonetheless, the simple calculation suggests that the $(3)^2\Sigma^+$ and $(4)^2\Sigma$ states cross near 5.4 eV above the ground electronic state, causing the rotational levels of the (4) state to effectively "disappear" from the expected pattern at N ~ 29 and above. Searches for transitions several N higher in frequency proved unsuccessful, as mentioned. In turn, the rotational levels of the (4) state are only observed at $N > 24$. Searches were conducted for lower transitions below $N = 24$ but were not found, focused again about a 100 MHz window of the expected pattern. It is curious that all vibrational satellite lines seem to be affected, even for $v = 13$ in the (3) state. The level populations must be depleted for $N = 29$ and higher through a collisional effect. Predissociation or interference phenomenon do not seem likely culprits. Predissociation fails to account for the disappearance at the same N levels irrespective of the vibrational level, and the appearance of the $(4)^2\Sigma^+$ transitions. Interference involves electronic, not pure rotational transitions. Some new effect or a combination of multiple effects must be occurring that needs further exploration with experimental and theorical work. Additional measurements and computations, including further lifetime calculations, are needed to fully unravel all the observed spectroscopic behavior in these two states of MgCl. Further work is in progress.

CONCLUSIONS

Using pure rotational spectroscopy, two new electronic states of MgCl have been experimentally observed, $(3)^2\Sigma^+$ and $(4)^2\Sigma^+$. These states appear to have unusually long lifetimes. Both states have been predicted by theory, in previous studies and with new, expanded computations at the CASPT2 and MRCISD+Q levels. The experimental data suggests strong nonadiabatic behavior in these states, as supported by the computations. The experimental data suggest that the $(3)^2\Sigma^+$ and $(4)^2\Sigma$ perturb each other near their $v = 7$ and 0 levels respectively, through an unexplained interaction. The electronic structure of MgCl is therefore nontrivial and involves strongly mixed character that challenge standard analysis techniques. Further investigation of relativistic and spin–orbit effects, and the influence of active space selection on electronic coupling, is clearly needed. A similar set of excited electronic states may also exist in MgBr and MgI and should be probed.

ASSOCIATED CONTENT

Supporting Information

The Supporting Information is available free of charge at https://pubs.acs.org/doi/10.1021/acs.jpca.4c05458.

Measured transitions (PDF)

AUTHOR INFORMATION

Corresponding Author

L. M. Ziurys − *Department of Chemistry and Biochemistry and Department of Astronomy and Steward Observatory, University of Arizona, Tucson, Arizona 85719, United States*; Email: lziurys@arizona.edu

Authors

T. J. Herman − *Department of Chemistry and Biochemistry, University of Arizona, Tucson, Arizona 85719, United States*

R. Ravi − *Department of Chemistry and Biochemistry, University of Arizona, Tucson, Arizona 85719, United States*; orcid.org/0000-0002-9204-6270

M. S. Schuurman − *Department of Chemistry and Biomolecular Sciences, National Research Council of Canada, Ottawa, ON K1A 0R6, Canada*

N. J. DeYonker − *Department of Chemistry, University of Memphis, Memphis, Tennessee 38152, United States*; orcid.org/0000-0003-0435-2006

R. W. Field − *Department of Chemistry, Massachusetts Institute of Technology, Cambridge, Massachusetts 02139, United States*; orcid.org/0000-0002-7609-4205

Complete contact information is available at: https://pubs.acs.org/10.1021/acs.jpca.4c05458

https://doi.org/10.1021/acs.jpca.4c05458
J. Phys. Chem. A XXXX, XXX, XXX−XXX

Notes

The authors declare no competing financial interest.

■ ACKNOWLEDGMENTS

The authors would like to thank Professor Lan Cheng (Johns Hopkins University) for helpful discussions. This research was supported by NSF grant CHE-2154121. L.M.Z. thanks RJS for the inspiring graduate work and extensive insight into molecular spectroscopy.

■ REFERENCES

(1) Shuman, E. S.; Barry, J. F.; DeMille, D. Laser Cooling of a Diatomic Molecule. *Nature* **2010**, *467* (7317), 820−823.

(2) Zhelyazkova, V.; Cournol, A.; Wall, T. E.; Matsushima, A.; Hudson, J. J.; Hinds, E. A.; Tarbutt, M. R.; Sauer, B. E. Laser Cooling and Slowing of CaF Molecules. *Phys. Rev. A* **2014**, *89* (5), No. 053416.

(3) Ladd, T. D.; Jelezko, F.; Laflamme, R.; Nakamura, Y.; Monroe, C.; O'Brien, J. L. Quantum Computers. *Nature* **2010**, *464* (7285), 45−53.

(4) DeMille, D. Quantum Computation with Trapped Polar Molecules. *Phys. Rev. Lett.* **2002**, *88* (6), No. 067901.

(5) Weitz, M. Towards Controlling Larger Quantum Systems: From Laser Cooling to Quantum Computing. *IEEE J. Quantum Electron.* **2000**, *36* (12), 1346−1357.

(6) Clark, J. L.; Rumbles, G. Laser Cooling in the Condensed Phase by Frequency Up-Conversion. *Phys. Rev. Lett.* **1996**, *76* (12), 2037−2040.

(7) Doppelbauer, M.; Wright, S. C.; Hofsäss, S.; Sartakov, B. G.; Meijer, G.; Truppe, S. Hyperfine-Resolved Optical Spectroscopy of the $A^2\Pi \leftarrow X^2\Sigma^+$ Transition in MgF. *J. Chem. Phys.* **2022**, *156* (13), 134301.

(8) Pelegrini, M.; Vivacqua, C. S.; Roberto-Neto, O.; Ornellas, F. R.; Machado, F. B. C. Radiative Transition Probabilities and Lifetimes for the Band Systems $A^2\Pi$ - $X^2\Sigma^+$ of the Isovalent Molecules BeF, MgF and CaF. *Braz. J. Phys.* **2005**, *35*, 950−956.

(9) Hao, Y.; Pašteka, L. F.; Visscher, L.; Aggarwal, P.; Bethlem, H. L.; Boeschoten, A.; Borschevsky, A.; Denis, M.; Esajas, K.; Hoekstra, S.; Jungmann, K.; Marshall, V. R.; Meijknecht, T. B.; Mooij, M. C.; Timmermans, R. G. E.; Touwen, A.; Ubachs, W.; Willmann, L.; Yin, Y.; Zapara, A. High accuracy theoretical investigations of CaF, SrF, and BaF and implications for laser-cooling. *J. Chem. Phys.* **2019**, *151* (3), No. 034302.

(10) Törring, T.; Ernst, W. E.; Kändler, J. Energies and Electric Dipole Moments of the Low Lying Electronic States of the Alkaline Earth Monohalides from an Electrostatic Polarization Model. *J. Chem. Phys.* **1989**, *90* (9), 4927−4932.

(11) Morgan, E.; Barrow, R. F. Rotational Analysis of the $A^2\Pi$−$X^2\Sigma^+$ System of MgCl. *Nature* **1961**, *192* (4808), 1182−1182.

(12) Herzberg, G. Spectra of Diatomic Molecules. In *Molecular Spectra & Molecular Structure*; Van Nostrand Reinhold: **1950**, *1*, 127.

(13) Liang, W.; Lu, G.; Yu, J. Molecular Dynamics Simulations of Molten Magnesium Chloride Using Machine-Learning-Based Deep Potential. *Adv. Theory Simul.* **2020**, *3* (12), No. 2000180.

(14) Yu, Y.; Liu, D.; Wu, H. Formation and Characteristics of Reaction Intermediates from the Fast Pyrolysis of NaCl- and MgCl2-Loaded Celluloses. *Energy Fuels* **2014**, *28* (1), 245−253.

(15) Xu, X.; Wang, X.; Li, P.; Li, Y.; Hao, Q.; Xiao, B.; Elsentriecy, H.; Gervasio, D. Experimental Test of Properties of KCl−$MgCl_2$ Eutectic Molten Salt for Heat Transfer and Thermal Storage Fluid in Concentrated Solar Power Systems. *J. Sol. Energy Eng.* **2018**, *140*, No. 051011.

(16) Cernicharo, J.; Guelin, M. Metals in IRC + 10216: Detection of NaCl, AlCl, and KCl, and Tentative Detection of Alf. *Astron. Astrophys.* **1987**, *183*, L10−L12.

(17) Bogey, M.; Demuynck, C.; Destombes, J. L. Millimeter Wave Spectrum of MgCl $X^2\Sigma^+$ and Isotopomers in Different Vibrational States. Determination of Mass-Invariant Parameters. *Chem. Phys. Lett.* **1989**, *155* (3), 265−268.

(18) Ohshima, Y.; Endo, Y. Fourier-Transform Microwave Spectroscopy of $^{24}Mg^{35}Cl$ Generated by Laser Ablation. *Chem. Phys. Lett.* **1993**, *213* (1), 95−100.

(19) Anderson, M. A.; Ziurys, L. M. Metal Hyperfine Structure in Magnesium Chloride. The Millimeter-Wave Spectrum of $^{25}MgCl$ and $^{26}MgCl$. *Chem. Phys. Lett.* **1994**, *224* (3), 381−390.

(20) Singh, M.; Ghodgaonkar, G. S.; Saksena, M. D. The $A^2\Pi$−$X^2\Sigma^+$ System of MgCl. *Can. J. Phys.* **1987**, *65* (12), 1594−1603.

(21) Hirao, T.; Bernath, P. F.; Fellows, C. E.; Gutterres, R. F.; Vervloet, M. High-Resolution Fourier Transform Study of MgCl: The $A^2\Pi$−$X^2\Sigma^+$ Band System. *J. Mol. Spectrosc.* **2002**, *212* (1), 53−56.

(22) Gutterres, R. F.; Dos Santos, R. F.; Fellows, C. E. Spectroscopic Study of the $^{24}Mg^{35}Cl$ and $^{24}Mg^{37}Cl$ $A^2\Pi$−$X^2\Sigma^+$ Band System. *Braz. J. Phys.* **2003**, *33*, 886−891.

(23) Singh, M.; Saksena, M. D.; Ghodgaonkar, G. S. The $B^2\Sigma^+$−$A^2\Pi_r$ System of MgCl. *Can. J. Phys.* **1988**, *66* (7), 570−575.

(24) Darji, A. B.; Sureshkumar, M. B.; Shah, P. M.; Shah, N. R. Rotational Analysis of 4730 Å Band of MgCl. *Pramana - J. Phys.* **1987**, *29* (3), 279−284.

(25) Drakes, J. A. Franck-Condon Factors of the MgCl (*A*-*X*) Band System. *Journal of Quantitative Spectroscopy and Radiative Transfer* **1995**, *54* (6), 1039−1044.

(26) Shafizadeh, N.; Rostas, J.; Taieb, G.; Bourguignon, B.; Prisant, M. G. Population Distribution of MgCl Formed from Mg+R-Cl Reactions. Determination of the Dissociation Energy of MgCl. *Chem. Phys.* **1990**, *142* (1), 111−122.

(27) Parlant, G.; Rostas, J.; Taieb, G.; Yarkony, D. R. On the Electronic Structure and Dynamical Aspects of the Predissociation of the $A^2\Pi_\Omega$ States of MgCl. A Rigorous Quantum Mechanical Treatment Incorporating Spin−Orbit and Derivative Coupling Effects. *J. Chem. Phys.* **1990**, *93* (9), 6403−6418.

(28) Wan, M.; Shao, J.; Gao, Y.; Huang, D.; Yang, J.; Cao, Q.; Jin, C.; Wang, F. Laser Cooling of MgCl and MgBr in Theoretical Approach. *J. Chem. Phys.* **2015**, *143* (2), No. 024302.

(29) Yang, Q.-S.; Li, S.-C.; Yu, Y.; Gao, T. Theoretical Study of the Feasibility of Laser Cooling the $^{24}Mg^{35}Cl$ Molecule Including Hyperfine Structure and Branching Ratios. *J. Phys. Chem. A* **2018**, *122* (11), 3021−3030.

(30) Wu, D.; Lin, C.; Wen, Y.; Xie, A.; Yan, B. Configuration Interaction Calculations on the Spectroscopic and Transition Properties of Magnesium Chloride*. *Chinese Phys. B* **2018**, *27* (8), No. 083101.

(31) Abu el kher, N.; El-Kork, N.; Korek, M. Electronic Structure with Rovibrational Calculations of the Magnesium Monohalides MgX and Their Cations MgX^+ (X = Cl, Br, and I). *ACS Omega* **2019**, *4* (26), 21741−21760.

(32) Ziurys, L. M.; Barclay, W. L.; Anderson, M. A.; Fletcher, D. A.; Lamb, J. W. A Millimeter/Submillimeter Spectrometer for High Resolution Studies of Transient Molecules. *Rev. Sci. Instrum.* **1994**, *65* (5), 1517−1522.

(33) Widmark, P.-O.; Persson, B. J.; Roos, B. O. Density Matrix Averaged Atomic Natural Orbital (ANO) Basis Sets for Correlated Molecular Wave Functions. *Theoretica Chimica Acta* **1991**, *79* (6), 419−432.

(34) Li Manni, G.; Fdez. Galván, I.; Alavi, A.; Aleotti, F.; Aquilante, F.; Autschbach, J.; Avagliano, D.; Baiardi, A.; Bao, J. J.; Battaglia, S.; Birnoschi, L.; Blanco-González, A.; Bokarev, S. I.; Broer, R.; Cacciari, R.; Calio, P. B.; Carlson, R. K.; Carvalho Couto, R.; Cerdán, L.; Chibotaru, L. F.; Chilton, N. F.; Church, J. R.; Conti, I.; Coriani, S.; Cuéllar-Zuquin, J.; Daoud, R. E.; Dattani, N.; Decleva, P.; de Graaf, C.; Delcey, M. G.; De Vico, L.; Dobrautz, W.; Dong, S. S.; Feng, R.; Ferré, N.; Filatov(Gulak), M.; Gagliardi, L.; Garavelli, M.; González, L.; Guan, Y.; Guo, M.; Hennefarth, M. R.; Hermes, M. R.; Hoyer, C. E.; Huix-Rotllant, M.; Jaiswal, V. K.; Kaiser, A.; Kaliakin, D. S.; Khamesian, M.; King, D. S.; Kochetov, V.; Krośnicki, M.; Kumaar, A. A.; Larsson, E. D.; Lehtola, S.; Lepetit, M.-B.; Lischka, H.; López Ríos, P.; Lundberg, M.; Ma, D.; Mai, S.; Marquetand, P.; Merritt, I. C. D.;

https://doi.org/10.1021/acs.jpca.4c05458
J. Phys. Chem. A XXXX, XXX, XXX−XXX

611 Montorsi, F.; Mörchen, M.; Nenov, A.; Nguyen, V. H. A.; Nishimoto,
612 Y.; Oakley, M. S.; Olivucci, M.; Oppel, M.; Padula, D.; Pandharkar,
613 R.; Phung, Q. M.; Plasser, F.; Raggi, G.; Rebolini, E.; Reiher, M.;
614 Rivalta, I.; Roca-Sanjuán, D.; Romig, T.; Safari, A. A.; Sánchez-
615 Mansilla, A.; Sand, A. M.; Schapiro, I.; Scott, T. R.; Segarra-Martí, J.;
616 Segatta, F.; Sergentu, D.-C.; Sharma, P.; Shepard, R.; Shu, Y.; Staab, J.
617 K.; Straatsma, T. P.; Sørensen, L. K.; Tenorio, B. N. C.; Truhlar, D.
618 G.; Ungur, L.; Vacher, M.; Veryazov, V.; Voß, T. A.; Weser, O.; Wu,
619 D.; Yang, X.; Yarkony, D.; Zhou, C.; Zobel, J. P.; Lindh, R. The
620 OpenMolcas Web: A Community-Driven Approach to Advancing
621 Computational Chemistry. *J. Chem. Theory Comput.* **2023**, *19* (20),
622 6933−6991.
623 (35) Prascher, B. P.; Woon, D. E.; Peterson, K. A.; Dunning, T. H.;
624 Wilson, A. K. Gaussian Basis Sets for Use in Correlated Molecular
625 Calculations. VII. Valence, Core-Valence, and Scalar Relativistic Basis
626 Sets for Li, Be, Na, and Mg. *Theor. Chem. Acc.* **2011**, *128* (1), 69−82.
627 (36) Peterson, K. A.; Dunning, T. H. Jr. Accurate Correlation
628 Consistent Basis Sets for Molecular Core−Valence Correlation
629 Effects: The Second Row Atoms Al−Ar, and the First Row Atoms
630 B−Ne Revisited. *J. Chem. Phys.* **2002**, *117* (23), 10548−10560.
631 (37) de Jong, W. A.; Harrison, R. J.; Dixon, D. A. Parallel Douglas−
632 Kroll Energy and Gradients in NWChem: Estimating Scalar
633 Relativistic Effects Using Douglas−Kroll Contracted Basis Sets. *J.*
634 *Chem. Phys.* **2001**, *114* (1), 48−53.
635 (38) Werner, H.-J.; Knowles, P. J.; Manby, F. R.; Black, J. A.; Doll,
636 K.; Heßelmann, A.; Kats, D.; Köhn, A.; Korona, T.; Kreplin, D. A.;
637 Ma, Q.; Miller, T. F. III; Mitrushchenkov, A.; Peterson, K. A.; Polyak,
638 I.; Rauhut, G.; Sibaev, M. The Molpro Quantum Chemistry Package.
639 *J. Chem. Phys.* **2020**, *152* (14), 144107.
640 (39) Shamasundar, K. R.; Knizia, G.; Werner, H.-J. A New Internally
641 Contracted Multi-Reference Configuration Interaction Method. *J.*
642 *Chem. Phys.* **2011**, *135* (5), No. 054101.
643 (40) Werner, H.; Knowles, P. J. An Efficient Internally Contracted
644 Multiconfiguration−Reference Configuration Interaction Method. *J.*
645 *Chem. Phys.* **1988**, *89* (9), 5803−5814.
646 (41) Brown, J. M.; Carrington, A. *Rotational Spectroscopy of Diatomic*
647 *Molecules*; Cambridge University Press: 2003.
648 (42) Pickett, H. M. The Fitting and Prediction of Vibration-Rotation
649 Spectra with Spin Interactions. *J. Mol. Spectrosc.* **1991**, *148*, 371−377.
650 (43) Lefebvre-Brion, H.; Field, R. W. *The Spectra and Dynamics of*
651 *Diatomic Molecules*: Revised and Enlarged ed.; Academic Press: 2004.

https://doi.org/10.1021/acs.jpca.4c05458
J. Phys. Chem. A XXXX, XXX, XXX−XXX